Title

Tunable Anisotropic Photon Emission from Self-Organized CsPbBr3 Perovskite Nanocrystals

Journal

Nano Letters, 17(7)

ISSN

1530-6984

Authors

Jurow, Matthew J
Lampe, Thomas
Penzo, Erika
et al.

Publication Date

2017-07-12

DOI

10.1021/acs.nanolett.7b02147

Peer reviewed

Tunable Anisotropic Photon Emission from Self Organized CsPbBr3 Perovskite Nanocrystals

Matthew J. Jurow[1,2], Thomas Lampe[3], Erika Penzo[1], Jun Kang[2], Matthew A. Koc[4], Thomas Zechel[3], Zachary Nett[4], Michael Brady[5], Lin-Wang Wang[3], A. Paul Alivisatos[2,4,6,7], Stefano Cabrini[1], Wolfgang Brütting[3], Yi Liu[1,2]**

[1] The Molecular Foundry, Lawrence Berkeley National Laboratory

Berkeley, CA 94720, USA

[2] Materials Sciences Division, Lawrence Berkeley National Laboratory

Berkeley, CA 94720, USA

[3]Institute of Physics, University of Augsburg

Augsburg 86135, Germany

[4]College of Chemistry, University of California, Berkeley

Berkeley, CA 94720 USA

[5]Advanced Light Source, Lawrence Berkeley National Laboratory

Berkeley, CA 94720, USA

[6] Department of Materials Science and Engineering, University of California, Berkeley

Berkeley, CA 94720 USA

[7]Kavli Energy NanoScience Institute,

Berkeley, CA 94720, USA

Yi Liu*: yliu@lbl.gov, telephone: 510-486-6287, fax: 510-486-7413

Wolfgang Brütting*: Wolfgang.bruetting@physik.uni-augsburg.de, telephone: ++49 (0)821-598-3403, fax: ++49 (0)821-598-3425

Abstract: We report controllable anisotropic light emission of photons originating from vertically aligned transition dipole moments in spun-cast films of $CsPbBr_3$ nanocubes. By depositing films of nanocrystals on pre-coated substrates we can control the packing density and resultant radiation pattern of the emitted photons. We develop a technical framework to calculate the average orientation of light emitters, i.e. the angle between the transition dipole moment vector (TDM) and the substrate. This model is applicable to any emissive material with a known refractive index. Theoretical modeling indicates that oriented emission originates from an anisotropic alignment of the valence band and conduction band edge states on the ionic crystal lattice, and demonstrates a general path to model the experimentally less accessible internal electric field of a nanosystem from the PL anisotropy. The uniquely accessible surface of the perovskite nanoparticles allows for perturbation of the normally isotropic emissive transition. The reported sensitive and tunable TDM orientation and control of emitted light will allow for applications of perovskite nanocrystals in a wide range of photonic technologies inaccessible to traditional light emitters.

KEYWORDS: perovskite, nanocrystal, oriented emission, $CsPbBr_3$

Since their initial synthesis, colloidal $CsPbBr_3$ perovskite nanocrystals have demonstrated a range of excellent optical properties including narrow, tunable emission, facile access to all wavelengths with minimal Stokes shifts, and photoluminescent quantum yields above 70% without embedding in a larger gap shell.[1-3] The controllable range of light emission from lead halide perovskite nanocrystals, spanning deep blue to the near infrared, allows efficient access to an exceptionally large color gamut, including pure white.[4, 5] The ionic nature of the crystal lattice and dynamic surface ligands allow for substantial control of nanocrystal morphology during synthesis, and facile procedures for the production of plates, cubes and wires have been developed.[6-13]

Compared to similar organic/inorganic hybrid perovskite materials, fully inorganic cesium based nanocrystals have lower defect densities, yielding larger charge carrier mobility values, no intra-gap states from uncoordinated surface atoms,[14-16] and improved stability in ambient conditions, making them promising materials for photovoltaics,[17-19] light emitting diodes,[17, 20-24] displays,[8, 11, 25, 26] lasers,[13, 18, 27, 28] and quantum optics.[5]

After the excellent initial reports about the emission behavior of individual nanocrystals by Rainò *et. al.* and Park *et. al.,* there has been relatively little investigation into the basic processes of photoluminescence in $CsPbBr_3$ nanocrystals.[29, 30] A thorough understanding of the mechanism of photon emission from these materials will be necessary to optimize perovskite nanocrystals for use in the most promising applications spaces.

The preferential alignment of the transition dipole moments of an emitter material has recently allowed for the production of extremely efficient optoelectronic devices. For example, this phenomenon enables the development of organic light emitting diodes close to 40% external quantum efficiency and improves the performance of organic photovoltaics.[31-36]

In order to achieve anisotropic light emission it is necessary to orient the transition dipole moment vector (TDM), a quantity describing the strength and direction of the electronic oscillation between the ground and emissive states of the emitting material.[37] It is important to note that even if the individual nanocrystals possess an oriented TDM, an ensemble of such nanocrystals randomly oriented in space will present isotropic photon emission when averaged over a wide sample area (ensemble averaging).

In this report we describe the unexpected observation of anisotropic light emission from assemblies of $CsPbBr_3$ nanocubes. We further find that by varying the substrate surface coatings we can control particle packing and in turn the fraction of power emitted perpendicular to the substrate. Experimental data and density functional theory modeling indicate that the uniquely tunable oriented photon emission stems from the relatively easily accessible surface of the perovskite nanocrystals allowing for the creation of an anisotropic band structure which, in turn, gives rise to a non-isotropic TDM orientation distribution. Developing control over the direction of emitted light from these earth abundant materials will improve LED efficiencies and open application spaces that benefit from oriented photon emission like luminescent solar concentrators, LCD backlights and photonic devices.[38-41]

Nanocrystal Synthesis and Characterization

Nanocubes were synthesized by a procedure adapted from the original report.[2] The measured absorption, emission and powder X-ray diffraction spectra were typical of $CsPbBr_3$ nanocubes.[42] Nanocrystals dispersed in toluene or spin coated onto glass display a sharp absorption peak at 495 nm (onset 519 nm) with a corresponding emission maximum at 512 nm (full width at half maximum of 20 nm), indicative of narrow particle size distribution, confirmed by transmission electron microscopy (TEM, see Supporting Information for details). Photoluminescent lifetimes

were non-monoexponential and exhibited a long-lived component, attributed to non-geminate recombination.[43] The transients were fit with a biexponential function, yielding values of 1.4 ns and 8.1 ns in toluene solution, consistent across all emissive wavelengths.

Nanocrystal Assemblies

To explore the relationship between the substrate, nanocube film formation properties and average orientation of light emitters, we deposited films of $CsPbBr_3$ nanocubes on glass slides coated with thin layers of SiO_2, indium tin oxide (ITO), polymerized hydrocarbon or polymerized fluorocarbon (**Figure 1**). Organic films were deposited onto glass substrates by polymerizing CH_4 or C_4F_8 in a plasma chamber. These materials were selected to produce a range of interactions between the substrate, the ligand shells, and the adjacent nanocube surface, as well as to provide a range of dielectric constants while allowing for rapid and accurate analysis of nanocube assemblies.

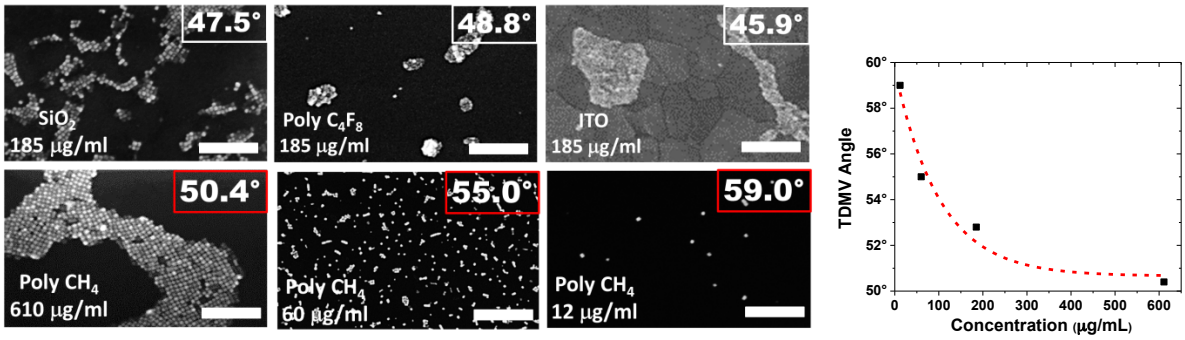

Figure 1. SEM images of films of $CsPbBr_3$ nanocubes self-assembled on coated surfaces. The angle between the substrate and the TDM are inset (scale bars: 200 nm). Spin casting from a range of nanocrystal concentrations onto different surfaces generally yields a consistent packing motif of aggregated nanocrystal superlattices. Light from these samples is emitted disproportionately in the plane of the substrate, with calculated TDM values (inset) relatively constant on SiO_2, polymerized fluorocarbon, and ITO surfaces. Samples deposited onto

polymerized methane coated substrates (bottom row) demonstrate the impact of diluting the nanocrystals solutions before spin coating on the final nanocrystal organization. By isolating the nanocrystals on the surface light emission becomes more oriented. The dashed red exponential fit line is a guide to illustrate the trend.

Particles spin coated from concentrated solutions in toluene organize into large self-assembled superlattices of nanocubes. Similar superlattice assemblies have demonstrated value as a precursor to 2D nanoplatelets upon pressurization.[44] Films were analyzed by grazing incidence small angle x-ray scattering (**Figure S13**) and feature a strong peak at 0.0449 $Å^{-1}$, corresponding to a superlattice periodicity of approximately 14 nm. This value implies an inter-cube spacing of 3 nm, indicating ligand intercalation between neighbors in the film. By coating the substrate on which we spin coat with a layer of polymerized hydrocarbon, the resulting superlattices become defect and grain boundary free over larger areas, as indicated by the growth of a second scattering peak at 0.0616 $Å^{-1}$ that corresponds to the diagonal plane spacing of ca. 10.2 nm.

By diluting the solution from which we spin coat onto the polymerized hydrocarbon surface layer we were able to effectively control the packing density of the cubes and neutralize the strong tendency to aggregate into superlattices. In this way we can reliably produce not only tiled monolayers microns across (concentration: 1.3 mg/mL in toluene), but also large rafts of cubes (600 μg/mL in toluene), agglomerates of less than ten cubes (60 μg/mL in toluene), and individual or coupled cubes separated by hundreds of nanometers (>10 μg/mL in toluene).

The packing motif of the perovskite nanocrystals deposited onto SiO_2, ITO or polymerized fluorocarbon are all comparable, exclusively featuring large islands of aggregated cubes separated by hundreds of nanometers. Changing the concentration of the solution from which

we spin coat has little impact on this assembly behavior, with samples spun cast from more concentrated solutions yielding larger islands of aggregates with smaller areas between rafts of cubes, and samples produced from extremely dilute solutions yielding comparably sized rafts of particles spaced farther apart. We were unable to separate individual cubes or isolate small bunches of cubes on these surfaces.

The ability to control the packing order of these nanocubes by altering the surface chemistry on which they are deposited likely results from the strong interaction between the C-H bond character on the hydrocarbon surface and the alkyl ligands surrounding the nanocrystals. These interactions are absent in all other tested substrates, including the analogous fluorous polymer that features only C-F groups and thus has limited affinity for the CH groups of the native nanocube ligands, leaving inter-particle interactions as the dominant organizing force resulting in surface aggregates. Such influence on packing order from interactions between substrate and shelling ligands has previously been observed in films of perovskites with modified ligand chemistries.[45]

Oriented Light Emission

Strongly quantum confined nanoscopic fluorophores have a complex two-dimensional TDM distribution, but commonly synthesized $CsPbBr_3$ nanocrystals, with a diameter of 10 nm and an excitonic Bohr radius of 7 nm, are very weakly quantum confined and primarily emit photons by excitonic recombination, a process which yields an isotropic TDM distribution in symmetric materials.[31, 46-51]

To measure the orientation of emitted photons from films of perovskite nanocubes we mounted the samples to a half-cylinder prism and measured the intensity of emitted light at all angles about the surface of the prism. The orientation of the TDM cannot be directly measured from the

emitted light intensity due to the orientation dependent transmission effects of the emitted light from a layered structure. To remove this geometry dependent anisotropy and resolve the quantum mechanical anisotropy of the TDM, we have modeled the emitted light dependence using a dipole radiation model in a one-dimensional micro-cavity as derived by Barnes et. al.[52] From this model, we can extract an alignment constant ζ (**Figure 2**, see supporting information for further details). This alignment constant, bounded from zero to one, is a quantification of the amount and angular distribution of radiated power for a particular emitting film. An alignment of the TDM perfectly parallel to the film surface is described by a value of zero, while perfect vertical alignment would be described by a value of one. Despite different refractive indices or TDM distributions, two emitting systems having the same alignment constant will show the same angular dependence of their radiations patterns. Additionally, confirming the assumption of a one-dimensional micro-cavity, we do not measure any alignment in the x-y plane due to the size of the excitation area (~1 mm^2) relative to the size of the emissive domain.

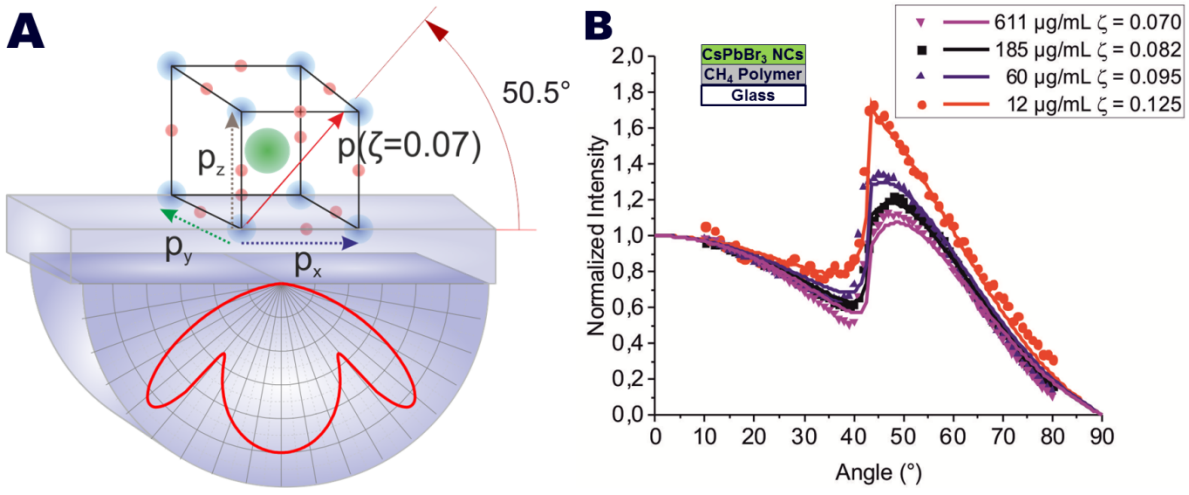

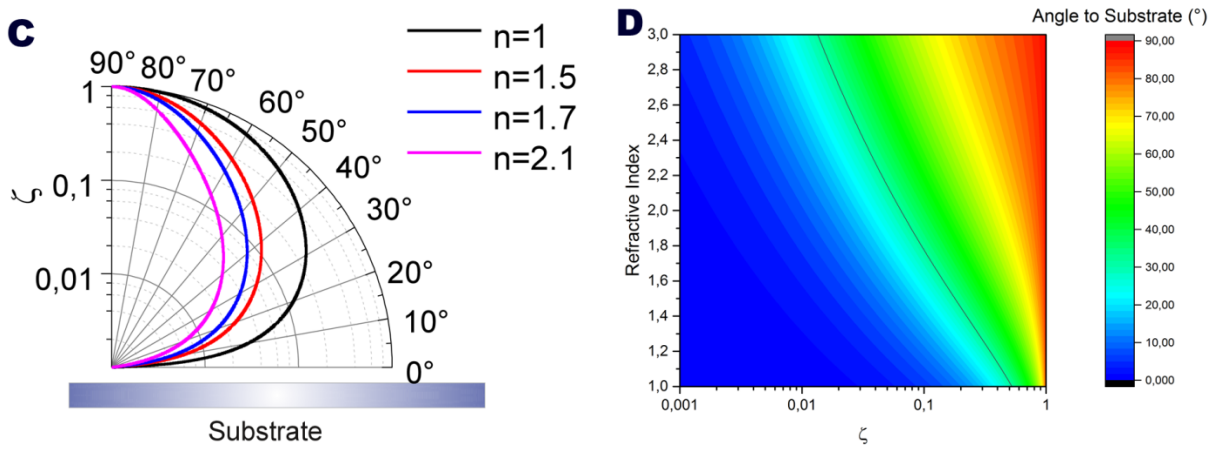

Figure 2. Measurements of the orientation of emitted light. (a) We extracted an alignment constant (ζ) from which we calculate the orientation of the average transition dipole moment vector (red arrow) from the pattern of light emitted (red line) through a prism. (b) Orientation measurement for films of $CsPbBr_3$ nanocubes whereby the alignment was controlled by changing the organization of the nanocrystals on the surface. The symbols are measured data from films of nanocrystals on hydrocarbon polymer coated surfaces to which the corresponding lines were fit. The fitted values correspond to TDM angles 50.5°, 53.0°, 55.0° and 59.1° with respect to the substrate surface. (c) The resulting TDM angle for a given value of ζ depends on the refractive index of the sample. The purple line depicts the expected behavior for the perovskite films. (d) From a given value of the alignment constant and the refractive index the resultant angle between the TDM and the substrate can be calculated for any emissive system. The black line indicates the values for isotropic emission, or a TDM angle of 35.2°, at any given refractive index.

Orientation data were collected from the photon emission of sub-monolayer films of perovskite nanocubes prepared from different dilutions on glass, polymerized fluorocarbon, polymerized hydrocarbon and ITO, as depicted in Figures 1 and 2. In addition to clearly

illustrating anisotropic light emission, the quality of the fit line with respect to the measured values demonstrates that the model, light emission originating from exciton recombination, is sound for the nanocrystals used.

Knowledge of the intrinsic refractive index is necessary to use the measured alignment constant ζ to determine the absolute TDM angle with respect to the substrate. Once the refractive index is known, we can state the relationship between the alignment constant, the refractive index (n) and the angle of the emissive TDM (φ) to the film substrate as Equation 1. This equation is applicable to any emissive material in this measurement geometry.

$$\varphi = \arcsin\left(\sqrt{\frac{n^4\zeta}{1+\zeta(n^4-1)}}\right) \quad \textbf{(1)}$$

The application of this model to emission from thin films enables the calculation of orientation distribution of the emissive TDM relative to the film plane from the measured radiation pattern of the material.[31, 53] If the system studied has more than one emissive TDM, the calculation will yield an average angle of the emission relative to the substrate.

When individual cubes were isolated, achieved experimentally by depositing on polymerized methane, the value of the alignment constant increases sharply from $\zeta = 0.07$ for densely packed rafts of cubes to $\zeta = 0.125$ for approximately isolated cubes (**Figure 1**). Films deposited on glass, SiO_2, ITO or polymerized fluorocarbon display a relatively constant anisotropy factor ranging from $\zeta = 0.051$ for sparse films on fluorous polymer to $\zeta = 0.058$ for sparse films on SiO_2, indicating that the packing motif and particle density exert a much larger impact on the direction of emitted photons than the physical properties of the substrate does.

In all measured cases light is found to be emitted with disproportionate intensity in the plane of the substrate, indicating that the TDM are localized vertically with respect to the film surface

(Figure 3). The large anisotropy value ($\zeta = 0.125$) measured from the segregated cubes on polymerized hydrocarbon corresponds to an average TDM value of 59°. The lowest value ($\zeta = 0.052$, $\varphi = 45.9°$) was measured from the film of $CsPbBr_3$ nanocubes on ITO. Thus, by changing the aggregation behavior of the cubes on the surface we can tune the orientation of emitted photons and the corresponding TDM angle by more than 13° (29%).

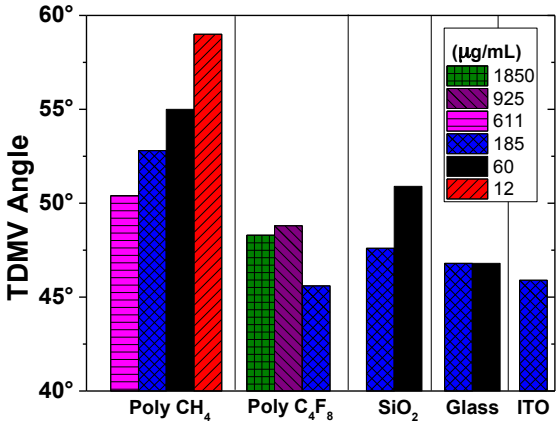

Figure 3. Calculated TDM angles for all samples measured. The surface coatings and concentrations from which the solutions were deposited are given in the legend.

We hypothesize that the observed oriented photon emission from $CsPbBr_3$ nanocubes is grounded in the accessible surface of the perovskite crystal. Oleate ligands are present on the nanocrystal surface and are necessary for colloidal stability, but unlike traditional quantum dots, complete coating of the nanocrystal surface is not typically required or achieved under normal synthetic conditions due to the high lability of the ligands.[10, 16] This allows for perturbation of the otherwise symmetric fluorophores by surface charges and contact between the bottom of the

cubes and the substrate, resulting in an anisotropy of the electronic transition between the ground and emissive excited states.

As a control experiment, films of 9.7 nm CdSe/CdS nanoparticles were spun cast onto similarly coated glass slides and the TDM angle of the assemblies measured in the same way. These particles are well passivated with a thick insulating shell, and should experience no comparable impacts from surface perturbations. Films were deposited from toluene solutions (10 μmol or 1 μmol) to form well-coated surfaces. All tested samples produced fully isotropic light emission patterns, indicative of symmetric transitions and/or randomly oriented particles (**Figure S10**).

Changes in the dielectric background around the nanocubes are likely responsible for the increasingly oriented emission seen from more isolated nanocubes. Higher dilutions of the nanocube solutions introduce more space between the nanocubes, reducing interaction between neighboring nanoparticles and enhancing the relative contribution of any perturbation induced by the substrate on the nanocrystal. Reducing the space between the crystals can also decrease the effective refractive index and therefore lead to a higher measured alignment constant.

Ab Initio Simulation

To understand the nature of the TDM anisotropy, we have used density functional theory (DFT) to study the possible scenarios from which an anisotropy may arise. Although it is difficult to ascribe the observed anisotropies in emission to any of the multiple possible scenarios, it is valuable to compare the effects on the TDM due to different plausible physical influences. The impact of the substrate on the nanocrystal assemblies and the impact of local defects or ions on the surfaces are two possible causes. To independently consider the potential impact of bringing an otherwise defect free perovskite nanocrystal into contact with a surface on

only one face, we constructed a (001) $CsPbBr_3$ surface with a 3 Å separation from a SiO_2 substrate (**Figure 4a**). The resulting calculation shows a pronounced charge redistribution, $\Delta\varrho$, defined by $\Delta\varrho=\varrho_{psk+sub}-\varrho_{psk}-\varrho_{sub}$, at the SiO_2/perovskite interface, comparable to previous reports in similar systems.[54] Here $\varrho_{psk+sub}$, ϱ_{psk} and ϱ_{sub} are the charge densities of the contacted system, isolated perovskite layer, and isolated substrate layer, respectively. The calculation indicates that bringing the perovskite crystal into contact with a silicon dioxide surface creates a redistribution of charge near the interface. The amount of the redistributed charge is calculated to be 0.006 e/Å^2 for SiO_2. Such a charge redistribution can potentially result in interface charging and creation of a local electric field perpendicular to the interface, breaking the symmetry of the cubic nanocrystal and leading to changes in both the valence band maximum (VBM) and conduction band minimum (CBM) states and producing the observed anisotropic TDM and resulting oriented light emission. This mechanism is expected to vary with the nature of the substrate, but the microscopic mechanism – asymmetric perturbation of one face of the nanocubes by the substrate – can be reasonably expected to apply to both inorganic and organic layers.

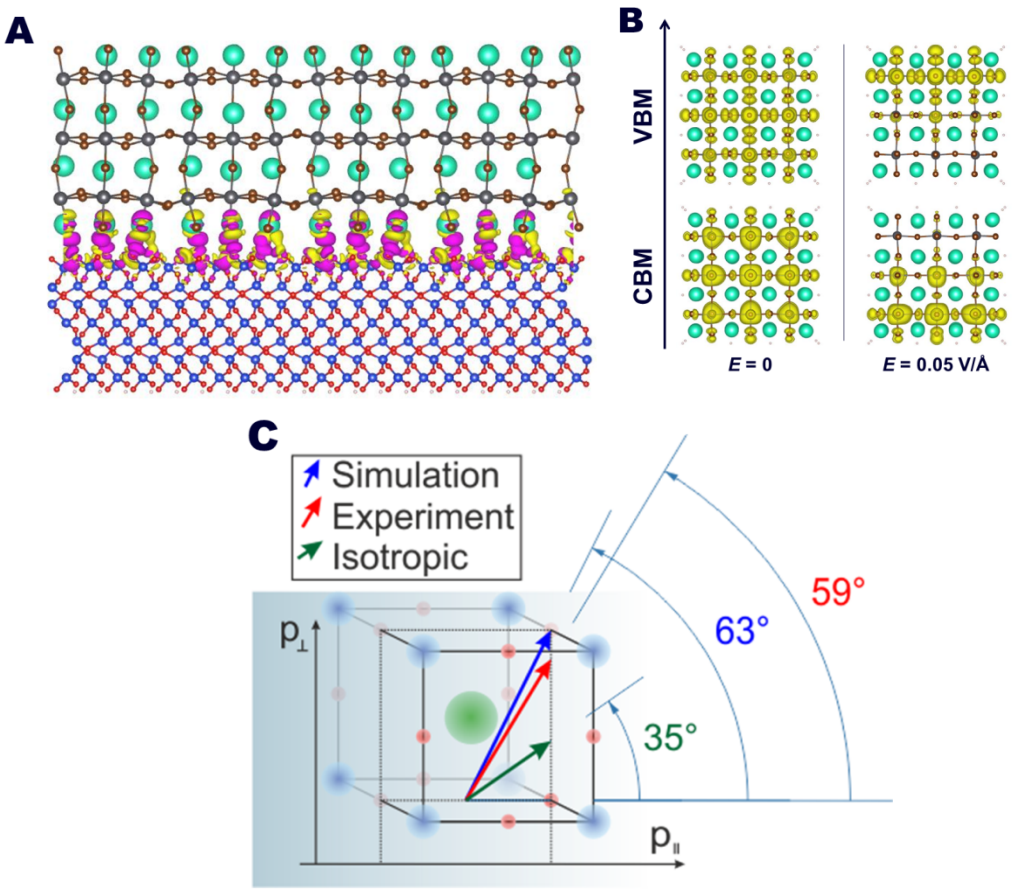

Figure 4. Density functional theory calculations illustrating the impact of electric fields on the TDM of $CsPbBr_3$ nanocrystals. (a) Modeling the effect of bringing the cubic perovskite lattice into approximate contact (3Å separation) with a silicon dioxide substrate shows a redistribution of the electron densities near the interface, introducing a small electrical field. (b) When this field is applied to the surface of an isolated perovskite nanocrystal the CBM and VBM surfaces become localized and the resulting TDM is calculated to transition from isotropic, which will yield a value of 35.2° by this measurement, to vertically oriented with an angle of 63° relative to the substrate. (c) Measured (red) and calculated (blue) angles as well as angle which would yield isotropic emission (green) are depicted on a single $CsPbBr_3$ unit cell.

To further demonstrate the above hypothesis, we constructed a $CsPbBr_3$ nanocube with [100] surface-termination as shown in **Figure 4b**. The Cs atoms at the corners and the edges of the nanocube are passivated by pseudohydrogen atoms to compensate for the excess electrons such that the nanocube exhibits a band gap. The CBM and VBM of a freestanding nanocube are isotropic, as shown in **Figure 4b**. The corresponding TDM, which is calculated by $|\langle\psi_{CBM}|i\nabla_\alpha|\psi_{VBM}\rangle|^2$ (α=x,y,z), is also isotropic, with Cartesian coordinates of (0.21, 0.21, 0.21) (x, y, and z, respectively) corresponding to an angle of 35.2° above the substrate plane.

We then impose an electric field of 0.05 V/Å, comparable to the effect calculated from the introduction of the substrate, along the z direction and recalculated the CBM and VBM distribution. The electric field introduces a physical separation of the CBM and VBM and creates an anisotropic TDM (**Figure 4b**). The calculated TDM has Cartesian components (.02, .02, .06) (x, y, and z, respectively) corresponding to a value of 64.8° above the surface of the substrate for a perfectly isolated single nanocrystal. As a result, a disproportionate amount of light would be expected to be emitted in the plane of the substrate. This result supports our hypothesis that the oriented light emission is caused by a local electric field and agrees with our observation of primarily horizontal light emission (**Figure 4c**). This technique demonstrates a general path to model the experimentally less accessible internal electric field of a nanosystem from the PL anisotropy.

Comparable effects have been observed in methyl ammonium lead halide films and nanocrystals by Stark spectroscopy, demonstrating induced alignment of dipoles at the perovskite/TiO_2 interface.[55] Similarly, Tauber *et. al.* used light polarization studies from individual methyl ammonium lead iodide ($MAPBI_3$) nanocrystals to observe polarized photoluminescence related to an alteration of band structure created by a distortion of the

tetragonal crystal lattice (a lower symmetry crystal phase than that of the $CsPbX_3$ type materials) that localizes the transition dipole moment vector along the Pb-I-Pb axis.[56] Additionally, a build-up of halide ions near the perovskite surface has been observed in $MAPBI_3$, introducing a local space charge.[57, 58]

In summary, we have observed strongly anisotropic light emission from solution-processed films of symmetric $CsPbBr_3$ perovskite nanocubes on a range of surfaces. We demonstrate that the degree of anisotropy of the emitted radiation can be controlled by modulating the interaction between the substrate and the nanocrystal surface to control particle spacing. By changing the packing of nanocrystals on the surface we can tune the average TDM orientation and thus the radiation pattern of emitted light.

Theoretical modeling shows that this effect can be created by the introduction of a small electric field on the surface of the crystal, which is easily accessible on $CsPbBr_3$ perovskite nanocrystals. This unusual control of photon emission in such an efficient fluorophore will allow the development of tunable materials for very specific applications in light emission and optical communication. Future work will explore this effect in perovskite nanocrystals with different morphologies, halide compositions, cations, ligand binding motifs, and especially physical environments. We are also exploring alternative measurement geometries to study specific emission wavelengths. Extreme orientations of emitted photons should be achievable and have the potential to yield highly efficient optoelectronic devices that rely on directional emission of light.

Supporting Information.

Synthetic details of all materials used, descriptions of sample deposition procedures and

measurement techniques, derivation of optical models and results, electron micrographs of all samples, GISAXS analysis of nanocrystal films.

The following files are available free of charge.

Electronic Supporting Information (PDF)

Corresponding Author

E-mail: yliu@lbl.gov

E-mail: Bruetting@physik.uni-augsburg.de

Author Contributions

The manuscript was written through contributions of all authors. All authors have given approval to the final version of the manuscript.

Funding Sources

Materials synthesis, sample preparation and analysis was supported by the Inorganic/Organic Nanocomposites Program (KC3104), and was performed at the Molecular Foundry, the X-ray scattering experiments were conducted at the Advanced Light Source (ALS), at Lawrence Berkeley National Laboratory, U.S. Department of Energy, Office of Science, Office of Basic Energy Sciences, Materials Sciences and Engineering Division, under Contract No. DE-AC02-05-CH11231. Z. Nett was supported by the Advanced Research Projects Agency – Energy (ARPA-E), U.S. Department of Energy, under Award Number DE-AR0000627.

T. Lampe, T. Zechel and W. Brütting acknowledge financial support by Bavaria California Technology Center (BaCaTeC), by the German Ministry for Education and Research (BMBF, Project no. 13N13664) and by Deutsche Forschungsgemeinschaft (DFG, Project no. Br 1728/18-1).

TDM, transition dipole moment vector; CBM, conduction band minimum; VBM, valence band maximum.

1. Wu, K.; Liang, G.; Shang, Q.; Ren, Y.; Kong, D.; Lian, T. *J. Am. Chem. Soc.* **2015,** 137, 12792-12795.
2. Protesescu, L.; Yakunin, S.; Bodnarchuk, M. I.; Krieg, F.; Caputo, R.; Hendon, C. H.; Yang, R. X.; Walsh, A.; Kovalenko, M. V. *Nano Lett.* **2015,** 15, 3692-3696.
3. Colella, S.; Mazzeo, M.; Rizzo, A.; Gigli, G.; Listorti, A. *J. Phys. Chem. Lett.* **2016,** 7, 4322-4334.
4. Yoon, H. C.; Kang, H.; Lee, S.; Oh, J. H.; Yang, H.; Do, Y. R. *ACS Appl. Mater. Interfaces* **2016,** 8, 18189-18200.
5. Sutherland, B. R.; Sargent, E. H. *Nat. Photonics* **2016,** 10, 295-302.
6. Shamsi, J.; Dang, Z.; Bianchini, P.; Canale, C.; Stasio, F. D.; Brescia, R.; Prato, M.; Manna, L. *J. Am. Chem. Soc.* **2016,** 138, 7240-7243.
7. Pan, A.; He, B.; Fan, X.; Liu, Z.; Urban, J. J.; Alivisatos, A. P.; He, L.; Liu, Y. *ACS Nano* **2016,** 10, 7943-7954.
8. Meyns, M.; Perálvarez, M.; Heuer-Jungemann, A.; Hertog, W.; Ibáñez, M.; Nafria, R.; Genç, A.; Arbiol, J.; Kovalenko, M. V.; Carreras, J.; Cabot, A.; Kanaras, A. G. *ACS Appl. Mater. Interfaces* **2016,** 8, 19579-19586.
9. Kim, Y.; Yassitepe, E.; Voznyy, O.; Comin, R.; Walters, G.; Gong, X.; Kanjanaboos, P.; Nogueira, A. F.; Sargent, E. H. *ACS Appl. Mater. Interfaces* **2015,** 7, 25007-25013.
10. De Roo, J.; Ibáñez, M.; Geiregat, P.; Nedelcu, G.; Walravens, W.; Maes, J.; Martins, J. C.; Van Driessche, I.; Kovalenko, M. V.; Hens, Z. *ACS Nano* **2016,** 10, 2071-2081.
11. Li, X.; Wu, Y.; Zhang, S.; Cai, B.; Gu, Y.; Song, J.; Zeng, H. *Adv. Funct. Mater.* **2016,** 26, 2435-2445.
12. Bekenstein, Y.; Koscher, B. A.; Eaton, S. W.; Yang, P.; Alivisatos, A. P. *J. Am. Chem. Soc.* **2015,** 137, 16008-16011.
13. Eaton, S. W.; Lai, M.; Gibson, N. A.; Wong, A. B.; Dou, L.; Ma, J.; Wang, L.-W.; Leone, S. R.; Yang, P. *Proc. Natl. Acad. Sci.* **2016,** 113, 1993-1998.
14. Yettapu, G. R.; Talukdar, D.; Sarkar, S.; Swarnkar, A.; Nag, A.; Ghosh, P.; Mandal, P. *Nano Lett.* **2016,** 16, 4838-4848.
15. ten Brinck, S.; Infante, I. *ACS Energy Lett.* **2016,** 1, 1266-1272.
16. Kang, J.; Wang, L.-W. *J. Phys. Chem. Lett.* **2017**, 8, 489-493.
17. Liang, J.; Wang, C.; Wang, Y.; Xu, Z.; Lu, Z.; Ma, Y.; Zhu, H.; Hu, Y.; Xiao, C.; Yi, X.; Zhu, G.; Lv, H.; Ma, L.; Chen, T.; Tie, Z.; Jin, Z.; Liu, J. *J. Am. Chem. Soc.* **2016,** 138, 15829-15832.

18. Veldhuis, S. A.; Boix, P. P.; Yantara, N.; Li, M.; Sum, T. C.; Mathews, N.; Mhaisalkar, S. G. *Adv. Mater.* **2016,** 28, 6804-6834.
19. Manser, J. S.; Christians, J. A.; Kamat, P. V. *Chem. Rev.* **2016,** 116, 12956-13008.
20. Xing, J.; Yan, F.; Zhao, Y.; Chen, S.; Yu, H.; Zhang, Q.; Zeng, R.; Demir, H. V.; Sun, X.; Huan, A.; Xiong, Q. *ACS Nano* **2016,** 10, 6623-6630.
21. Yuan, M.; Quan, L. N.; Comin, R.; Walters, G.; Sabatini, R.; Voznyy, O.; Hoogland, S.; Zhao, Y.; Beauregard, E. M.; Kanjanaboos, P.; Lu, Z.; Kim, D. H.; Sargent, E. H. *Nat. Nanotechnol.* **2016,** 11, 872-877.
22. Wang, R.; Shang, Y.; Kanjanaboos, P.; Zhou, W.; Ning, Z.; Sargent, E. H. *Energy Environ. Sci.* **2016,** 9, 1130-1143.
23. Pan, J.; Quan, L. N.; Zhao, Y.; Peng, W.; Murali, B.; Sarmah, S. P.; Yuan, M.; Sinatra, L.; Alyami, N. M.; Liu, J.; Yassitepe, E.; Yang, Z.; Voznyy, O.; Comin, R.; Hedhili, M. N.; Mohammed, O. F.; Lu, Z. H.; Kim, D. H.; Sargent, E. H.; Bakr, O. M. *Adv. Mater.* **2016**, 28, 8718-8725.
24. Wang, J.; Wang, N.; Jin, Y.; Si, J.; Tan, Z.-K.; Du, H.; Cheng, L.; Dai, X.; Bai, S.; He, H.; Ye, Z.; Lai, M. L.; Friend, R. H.; Huang, W. *Adv. Mater.* **2015,** 27, 2311-2316.
25. Palazon, F.; Di Stasio, F.; Akkerman, Q. A.; Krahne, R.; Prato, M.; Manna, L. *Chem. Mater.* **2016,** 28, 2902-2906.
26. Yoon, H. C.; Kang, H.; Lee, S.; Oh, J. H.; Yang, H.; Do, Y. R. *ACS Appl. Mater. Interfaces* **2016,** 8, 18189-18200.
27. Wang, Y.; Li, X.; Song, J.; Xiao, L.; Zeng, H.; Sun, H. *Adv. Mater.* **2015,** 27, 7101-7108.
28. Castañeda, J. A.; Nagamine, G.; Yassitepe, E.; Bonato, L. G.; Voznyy, O.; Hoogland, S.; Nogueira, A. F.; Sargent, E. H.; Cruz, C. H. B.; Padilha, L. A. *ACS Nano* **2016,** 10, 8603-8609.
29. Rainò, G.; Nedelcu, G.; Protesescu, L.; Bodnarchuk, M. I.; Kovalenko, M. V.; Mahrt, R. F.; Stöferle, T. *ACS Nano* **2016,** 10, 2485-2490.
30. Park, Y.-S.; Guo, S.; Makarov, N. S.; Klimov, V. I. *ACS Nano* **2015,** 9, 10386-10393.
31. Jurow, M. J.; Mayr, C.; Schmidt, T. D.; Lampe, T.; Djurovich, P. I.; Brutting, W.; Thompson, M. E. *Nat. Mater.* **2016,** 15, 85-91.
32. Kim, K.-H.; Moon, C.-K.; Lee, J.-H.; Kim, S.-Y.; Kim, J.-J. *Adv. Mater.* **2014,** 26, 3844-3847.
33. Kim, S.-Y.; Jeong, W.-I.; Mayr, C.; Park, Y.-S.; Kim, K.-H.; Lee, J.-H.; Moon, C.-K.; Brütting, W.; Kim, J.-J. *Adv. Funct. Mater.* **2013,** 23, 3896-3900.
34. Kim, K.-H.; Liao, J.-L.; Lee, S. W.; Sim, B.; Moon, C.-K.; Lee, G.-H.; Kim, H. J.; Chi, Y.; Kim, J.-J. *Adv. Mater.* **2016,** 28, 2526-2532.
35. Yokoyama, D.; Qiang Wang, Z.; Pu, Y.-J.; Kobayashi, K.; Kido, J.; Hong, Z. *Sol. Energy Mater. Sol. Cells* **2012,** 98, 472-475.
36. Hörmann, U.; Lorch, C.; Hinderhofer, A.; Gerlach, A.; Gruber, M.; Kraus, J.; Sykora, B.; Grob, S.; Linderl, T.; Wilke, A.; Opitz, A.; Hansson, R.; Anselmo, A. S.; Ozawa, Y.; Nakayama, Y.; Ishii, H.; Koch, N.; Moons, E.; Schreiber, F.; Brütting, W. *J. Phys. Chem. C* **2014,** 118, 26462-26470.
37. Turro, N. J., *Modern molecular photochemistry of organic molecules*. University Science Books: Sausalito, Calif., 2010.
38. Dirin, D. N.; Protesescu, L.; Trummer, D.; Kochetygov, I. V.; Yakunin, S.; Krumeich, F.; Stadie, N. P.; Kovalenko, M. V. *Nano Lett.* **2016,** 16, 5866-5874.
39. Jang, E.; Jun, S.; Jang, H.; Lim, J.; Kim, B.; Kim, Y. *Adv. Mater.* **2010,** 22, 3076-3080.
40. Zhu, R.; Kumar, A.; Yang, Y. *Adv. Mater.* **2011,** 23, 4193-4198.

41. Meinardi, F.; Ehrenberg, S.; Dhamo, L.; Carulli, F.; Mauri, M.; Bruni, F.; Simonutti, R.; Kortshagen, U.; Brovelli, S. *Nat. Photonics* **2017,** 11, 177-185.
42. Cottingham, P.; Brutchey, R. L. *Chem. Commun.* **2016,** 52, 5246-5249.
43. Pavliuk, M. V.; Fernandes, D. L. A.; El-Zohry, A. M.; Abdellah, M.; Nedelcu, G.; Kovalenko, M. V.; Sá, J. *Adv. Opt. Mater.* **2016,** 4, 2004-2008.
44. Nagaoka, Y.; Hills-Kimball, K.; Tan, R.; Li, R.; Wang, Z.; Chen, O. *Adv. Mater.* **2017**, 29, 1606666.
45. Yassitepe, E.; Yang, Z.; Voznyy, O.; Kim, Y.; Walters, G.; Castañeda, J. A.; Kanjanaboos, P.; Yuan, M.; Gong, X.; Fan, F.; Pan, J.; Hoogland, S.; Comin, R.; Bakr, O. M.; Padilha, L. A.; Nogueira, A. F.; Sargent, E. H. *Adv. Funct. Mater.* **2016,** 26, 8757-8763.
46. Brokmann, X.; Coolen, L.; Hermier, J.-P.; Dahan, M. *Chem. Phys.* **2005,** 318, 91-98.
47. Chung, I.; Shimizu, K. T.; Bawendi, M. G. *Proc. Natl. Acad. Sci.* **2003,** 100, 405-408.
48. Vanhelmont, F. W. M.; Strouse, G. F.; Güdel, H. U.; Stückl, A. C.; Schmalle, H. W. *J. Phys. Chem. A* **1997,** 101, 2946-2952.
49. Brokmann, X.; Coolen, L.; Dahan, M.; Hermier, J. P. *Phys. Rev. Lett.* **2004,** 93, 107403.
50. Swarnkar, A.; Chulliyil, R.; Ravi, V. K.; Irfanullah, M.; Chowdhury, A.; Nag, A. *Angew. Chem., Int. Ed.* **2015,** 54,15424-15428.
51. Butkus, J.; Vashishtha, P.; Chen, K.; Gallaher, J. K.; Prasad, S. K. K.; Metin, D. Z.; Laufersky, G.; Gaston, N.; Halpert, J. E.; Hodgkiss, J. M. *Chem. Mater.* **2017,** 29, 3644-3652.
52. Barnes, W. L. *J. Mod. Opt.* **1998,** 45, 661-699.
53. Frischeisen, J.; Yokoyama, D.; Endo, A.; Adachi, C.; Brütting, W. *Org. Electron.* **2011,** 12, 809-817.
54. Mosconi, E.; Ronca, E.; De Angelis, F. *J. Phys. Chem. Lett.* **2014,** 5, 2619-2625.
55. Roiati, V.; Mosconi, E.; Listorti, A.; Colella, S.; Gigli, G.; De Angelis, F. *Nano Lett.* **2014,** 14, 2168-2174.
56. Täuber, D.; Dobrovolsky, A.; Camacho, R.; Scheblykin, I. G. *Nano Lett.* **2016,** 16, 5087-5094.
57. Tress, W.; Marinova, N.; Moehl, T.; Zakeeruddin, S. M.; Nazeeruddin, M. K.; Gratzel, M. *Energy Environ. Sci.* **2015,** 8, 995-1004.
58. Xiao, Z.; Yuan, Y.; Shao, Y.; Wang, Q.; Dong, Q.; Bi, C.; Sharma, P.; Gruverman, A.; Huang, J. *Nat. Mater.* **2015,** 14, 193-198.

For TOC only: